

Article

Magnetized and Magnetically Charged Particles Motion around Regular Bardeen Black Hole in 4D Einstein Gauss–Bonnet Gravity

Javlon Rayimbaev ^{1,2,3,4,5,6} , Dilshodbek Bardiev ⁷ , Farrux Abdulxamidov ⁸, Ahmadjon Abdujabbarov ^{1,3,4,8,9}  and Bobomurat Ahmedov ^{1,4,9,*} 

- ¹ Ulugh Beg Astronomical Institute, Astronomy St. 33, Tashkent 100052, Uzbekistan
 - ² College of Engineering, Akfa University, Kichik Halqa Yuli Street 17, Tashkent 100095, Uzbekistan
 - ³ Power Engineering Faculty, Tashkent State Technical University, Tashkent 100095, Uzbekistan
 - ⁴ Faculty of Physics, National University of Uzbekistan, Tashkent 100174, Uzbekistan
 - ⁵ Institute of Fundamental and Applied Research, National Research University TIAME, Kori Niyoziy 39, Tashkent 100000, Uzbekistan
 - ⁶ Engineering Physics, Samarkand State University, University Avenue 15, Samarkand 140104, Uzbekistan
 - ⁷ Research Centre for Theoretical Physics and Astrophysics, Institute of Physics, Silesian University in Opava, Bezručovo nám. 13, CZ-74601 Opava, Czech Republic
 - ⁸ Institute of Nuclear Physics, Ulugbek 1, Tashkent 100214, Uzbekistan
 - ⁹ Department of Physics, Tashkent Institute of Irrigation and Agricultural Mechanization Engineers, Kori Niyoziy, 39, Tashkent 100000, Uzbekistan
- * Correspondence: ahmedov@astrin.uz



Citation: Rayimbaev, J.; Bardiev, D.; Abdulxamidov, F.; Abdujabbarov, A.; Ahmedov, B. Magnetized and Magnetically Charged Particles Motion around Regular Bardeen Black Hole in 4D Einstein Gauss–Bonnet Gravity. *Universe* **2022**, *8*, 549. <https://doi.org/10.3390/universe8100549>

Academic Editors: Daniela D. Doneva and Roman Konoplya

Received: 13 August 2022

Accepted: 17 October 2022

Published: 21 October 2022

Publisher's Note: MDPI stays neutral with regard to jurisdictional claims in published maps and institutional affiliations.

Abstract: In this paper, we study the horizon properties and scalar invariants of the spacetime around a regular black hole (BH) in 4D Einstein Gauss-Bonnet (4D EGB) gravity. It is observed that the presence of both Gauss-Bonnet (GB) coupling and magnetic charge parameters causes the shrinking of the outer horizon. We find that the range of the GB parameter $\alpha/M^2 \in (-0.15869, 1)$, and the extreme value of magnetic charge reaches up to $g_{\text{extr}} = 0.886M$, which allows for the existence of a BH horizon, while it is $g_{\text{extr}} = 0.7698M$ for pure Bardeen BH. We also investigate the dynamics of magnetized particles around the magnetically charged Bardeen BH, assuming the particle's motion occurs in the equatorial plane in the proper observation frame, and the direction of the magnetic dipole moment of the particles is always kept radially and its magnitude is constant. Moreover, the dynamics of magnetically charged particles are also studied, and it is shown that both the energy and angular momentum of the particles corresponding to circular orbits increases with the increase of their magnetic charge. Finally, we also study collisions of magnetized, electrically neutral, and magnetically charged particles around the Bardeen BHs, where we provide analyses of critical angular momentum that may allow collision of the particles near-horizon radius, producing enormous values of center of mass energy of the collisions.

Keywords: black holes; magnetic fields; magnetized particles; relativistic stars; orbits

PACS: 04.50.-h; 04.40.Dg; 97.60.Gb



Copyright: © 2022 by the authors. Licensee MDPI, Basel, Switzerland. This article is an open access article distributed under the terms and conditions of the Creative Commons Attribution (CC BY) license (<https://creativecommons.org/licenses/by/4.0/>).

1. Introduction

General Relativity (GR) proposed by Einstein in 1915 was the next modification of the gravity theories and has been successfully tested in 1919 using a solar eclipse. Since that day, this theory has been considered as a main theory describing the gravitational interaction in both strong and weak field regimes. Moreover, general relativity has been successfully tested in both weak and strong field regimes using a large number of experiments and observations [1–4]. On the other hand, several fundamental problems such as the physical singularity at the center of the Schwarzschild BHs ($r = 0$), ring singularity problem of the

Kerr BH solution, inconsistency with quantum field theory, etc., which occur in the frame of GR itself, provide evidence for the theory to become a unique theory of gravity. In order to avoid these issues and to step forward in the direction of obtaining a unified theory of interactions, one may need to formulate and explore modifications or/and alternative theories of gravity.

Higher dimensional theories of gravity help us to understand the nature of the gravitational interaction. One of the interesting extensions of the four-dimensional Einstein gravity to higher dimensions is called Einstein–Gauss–Bonnet (EGB) theory defined in $D > 4$ dimensional spacetime. According to the Lovelock theorem, the Gauss–Bonnet extension will be vanished in $D = 4$ dimensional spacetime [5]. In order to keep the Gauss–Bonnet term in $D = 4$ dimensional spacetime, the authors of [6] have proposed an approach based on the rescaling of the Gauss–Bonnet term by the factor $1/(D - 4)$. Using this approach, one may obtain a 4D in the framework of the EGB theory.

Gravitational collapse of the spherical homogeneous dust in 4D EGB gravity has been studied in [7]. Quasilinear modes of compact objects in 4D EGB gravity have been studied by the authors of [8]. The stability of the solution of 4d EGB gravity has been discussed in Ref. [9]. A review of the dynamics of the particles with non-zero spin around black hole (BH) in 4D EGB theory can be found [10,11]. Other properties of 4D EGB gravity and corresponding solutions including horizon structure and optical properties can be found in Refs. [12–26]. On the other hand, it is worth noting that the approach discussed in [6] in order to obtain four-dimensional theory of EGB modification has been questioned in several works [27–30], arguing that the solution and theory in $D = 4$ is not well-defined. Here is our main aim to test the theory and corresponding solution using the analysis of dynamics of particles with the non-zero magnetic charge and dipole around a regular black hole in 4D EGB gravity.

Testing gravity models using observational tools, particularly, using X-ray observation data from astrophysical objects, may provide constraints on the physical parameters of the theory and corresponding solutions [31–34]. At the same time, dynamics of the test particle can be also considered as a useful tool in developing new tests of metric theories of gravity [35,36]. General relativistic solutions describing the BHs do not have a proper magnetic field. Thus, in order to describe the electromagnetic field around the black hole, one may consider the latter immersed in an external magnetic field [37]. The electromagnetic field structure will be modified due to spacetime curvature, and this affects the charged particle dynamics (see, e.g., Refs. [38–54]). On the other hand, one may apply the dynamics of particles with non-zero magnetic charge or/and dipole around a compact object in the presence of electromagnetic field to astronomical observation from the compact objects [25,55–66].

In this study, we plan to explore the spacetime properties as well as particle dynamics around regular Bardeen BH within the 4D EGB gravity. The paper is organized as follows: Section 2 is devoted to studying the properties of the spacetime around regular Bardeen BH in 4D EGB gravity, including horizon structure and curvature scalars.

Section 3 is devoted to the analysis of dynamics of the magnetized particles around regular Bardeen BH in the framework of 4D EGB gravity. Magnetically charged particle motion has been discussed in Section 4. In Section 5, we discuss the magnetized particle's collision. We conclude and summarize the results of the paper in Section 6. In this paper, we use a space-like signature $(-, +, +, +)$ for the spacetime and geometrized unit of the system where $G = 1 = c$. Latin (Greek) indices run from 1 (0) to 3.

2. Regular Bardeen BH in 4D EGB Gravity

Consider the properties of the spacetime around static regular Bardeen BH in the 4-EGB gravity with re-scaled Gauss–Bonnet coupling constant, $\alpha/(D - 4)$ including minimally

coupled with the nonlinear electrodynamics (NED) in D -dimensional spacetime. The action for this case has the form [26]

$$\mathcal{S}_G = \frac{1}{16\pi} \int d^D x \sqrt{-\bar{g}} \left(R + \frac{\alpha}{D-4} L_{GB} + L(F) \right), \tag{1}$$

where $L(F)$ is the Lagrangian density, which is the function of the electromagnetic field invariant $F = F_{\mu\nu}F^{\mu\nu}/4$, $F_{\mu\nu} = \partial_\mu A_\nu - \partial_\nu A_\mu$ is the electromagnetic field tensor for the gauge potential A_μ , and L_{GB} is the Gauss–Bonnet correction of form

$$L_{GB} = R^{\mu\nu\rho\sigma}R_{\mu\nu\rho\sigma} - 4R^{\mu\nu}R_{\mu\nu} + R^2, \tag{2}$$

\bar{g} is the determinant of the metric tensor $g_{\mu\nu}$ and R , $R_{\mu\nu}$ and $R^{\mu}_{\nu\gamma\sigma}$ are Ricci scalar, Ricci tensor and Reimann tensor, respectively, the gravitational field equations can be found varying the action (1) in the following form

$$G_{\mu\nu} + \frac{\alpha}{D-4} H_{\mu\nu} = T_{\mu\nu}, \tag{3}$$

where

$$G_{\mu\nu} = R_{\mu\nu} - \frac{1}{2}g_{\mu\nu}R, \tag{4}$$

$$H_{\mu\nu} = 2(RR_{\mu\nu} - 2R_{\mu\sigma}R^\sigma_\nu - 2R_{\mu\nu\sigma\rho}R^{\sigma\rho} - R_{\mu\sigma\delta\rho}R^{\sigma\delta\rho}) - \frac{1}{2}g_{\mu\nu}L(F), \tag{5}$$

$$T_{\mu\nu} = 2 \left[L_F F_{\mu\sigma}F^\sigma_\nu - \frac{1}{4}g_{\mu\nu}L(F) \right]. \tag{6}$$

The Lagrangian density for the NED field in the D -dimensional spacetime has the following form [26]

$$L(F) = \frac{(D-1)(D-2)\mu^{D-3}}{4g^{D-3}} \left(\frac{\sqrt{2g^2F}}{1 + \sqrt{2g^2F}} \right)^{\frac{2D-3}{D-2}}, \tag{7}$$

with

$$F = \frac{g^{2(D-3)}}{2r^{2(D-2)}}, \tag{8}$$

where g is the magnetic charge governed by the NED field.

The solution of Equation (3) with the Lagrangian of form (7) in 4D EGB theory when $D = 4$ has the following form [26]

$$ds^2 = -f(r)dt^2 + \frac{1}{f(r)}dr^2 + d\Omega^2, \tag{9}$$

with

$$f(r) = 1 + \frac{r^2}{2\alpha} \left(1 \pm \sqrt{1 + \frac{8M\alpha}{(r^2 + g^2)^{\frac{3}{2}}}} \right), \tag{10}$$

where α is the GB coupling parameter and M is the total mass of the regular BH. In this work, we use the “-” sign for the function in Equation (10) due to the fact that in the limit of $\alpha \rightarrow 0$, this solution tends to the regular Bardeen BH in general relativity [67], which turns to the Schwarzschild BH solution in GR when $g = \alpha = 0$. Furthermore, in our analytical and numerical calculation and producing plots, we use $\alpha/M^2 \rightarrow \alpha$.

The non-zero components of the four-potential of the electromagnetic field surrounding the BH are [62,68]

$$A_\mu = (A_t^*, 0, 0, A_\phi), \quad A_t^* = -\frac{ig}{r}, \quad A_\phi = g\cos\theta. \tag{11}$$

2.1. Event Horizon Structure of the Regular Bardeen BH in 4D-EGB Gravity

First, we study the event horizon properties of the spacetime around regular Bardeen BH governed by the line element given in Equation (9).

In Figure 1, we have shown the radial dependence of the lapse function $f(r)$ in Equation (10) for the different values of parameters α and g . The left panel corresponds to the fixed value of $\alpha = -0.1$ and the right one corresponds to the fixed value of $\alpha = 0.3$. The values of the lapse function $f(r)$ intersect with the zero lines at two points which correspond to the inner and outer horizons. When $\alpha \geq 0$, as the magnetic charge increases, the distance between these horizons decreases, and when it reaches some extreme value, the inner and outer horizons converge to form a single horizon. The extreme values of magnetic charge depend on the GB parameter α , and we will be back to the relationship later in this subsection. The analysis of the solution of the equation $f(r) = 0$ shows that there is an extreme value of magnetic charge g_{ext} and:

- (i) There are two (inner and outer) event horizons corresponding to the values of magnetic charge $g < g_{ext}$;
- (ii) There is one event horizon corresponding to the value of magnetic charge $g = g_{ext}$ and one has the extremely charged regular Bardeen BH;
- (iii) There is no event horizon corresponding to the values of magnetic charge, $g > g_{ext}$ and one deals with a no-horizon strong gravitating regular object.

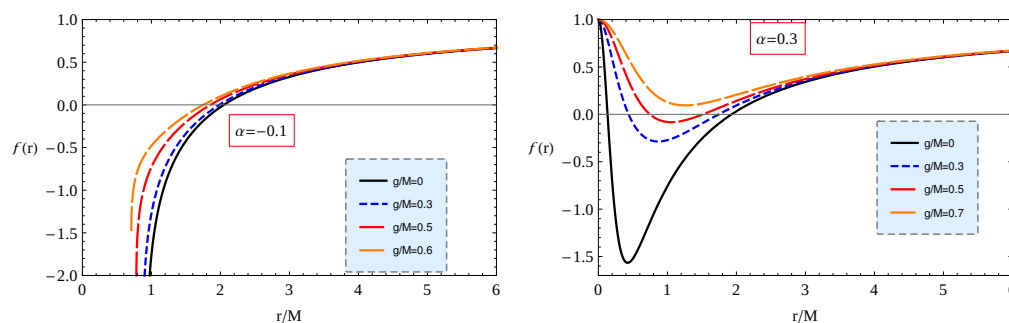


Figure 1. The radial dependence of the lapse function $f(r)$ for the different values of parameter. **left** panel is for $\alpha = 0.1$ and the **right** one is for $\alpha = 0.3$.

In order to study the effects of the NED charge and GB coupling parameters on the radius of the outer horizon, one may use the conditions $g_{rr} \rightarrow \infty, g^{rr} = 0$ leading to the equivalent equation $f(r) = 0$.

The dependence of the outer event horizon from the magnetic charge of regular Bardeen BH (left panel) and the GB coupling parameter (right panel) are shown in Figure 2, respectively. One can see that the extreme values of the charge g corresponding to the case with single horizon decreases with the increase of the GB coupling parameter. Moreover, the increase of the charge parameter causes the decrease of the upper value of α parameter. In order to find the extreme value of the charge g_{ext} and the corresponding value of the radius of event horizon r_h^{ext} of the extreme magnetically charged regular BH, one may solve the system of equations

$$f(r) = 0, f'(r) = 0.$$

Possible values of the parameters α and g corresponding to the extreme regular Bardeen BHs in 4D EGB theory are shown in Figure 3. In this plot, the space $\alpha - g$ is divided into two regions corresponding to BH and no-horizon objects. Numerical analysis shows that the coupling parameter α lies in the range of, $\alpha/M^2 \in (-0.15869, 1)$ and the values of the magnetic charge take the values in the range $g/M \in (0, 0.88625)$. The radius of the event horizon of the extreme regular BH in 4D EGB gravity takes the values in the range $r_h/M \in (0.840291, 2)$. One may also obtain that at $\alpha/M^2 \simeq -0.15869$ and $g \simeq 0.886247M$, the outer horizon takes the value $(r_h)_{min} \simeq 0.840291M$. Moreover, from Figure 3, one may

observe that in the limit when $\alpha = 0$, the extreme magnetic charge of the Bardeen BH has the value $g_{\text{ext}} = 4M/(3\sqrt{3}) \simeq 0.7698M$.

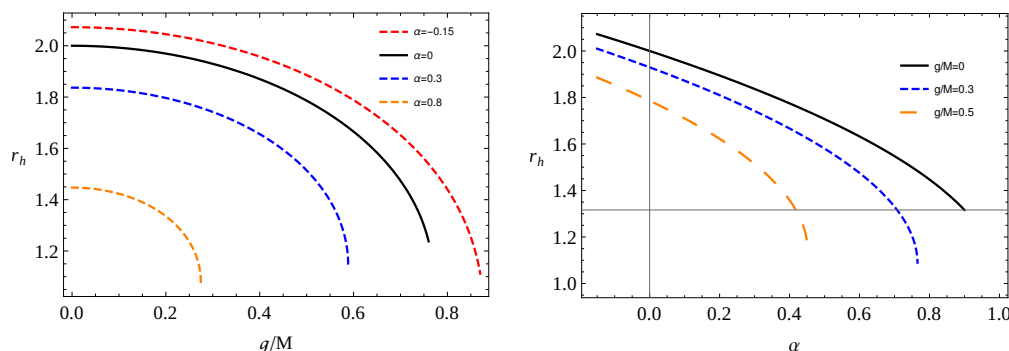


Figure 2. The dependence of outer event horizon on the parameters g (left panel) and α (right panel). Here, the radius of horizon of r_h is normalized in M .

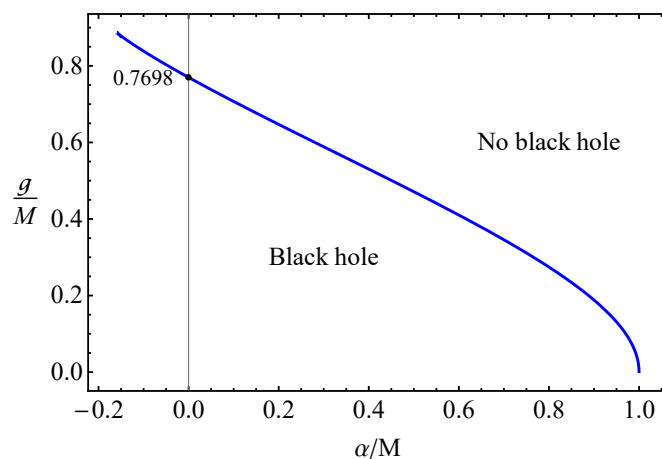


Figure 3. Relations between the values of parameter α and the BH charge g for the existence of the Bardeen BH horizon.

2.2. Curvature Scalars

The curvature invariants such as the Ricci scalar $R = g^{\mu\nu} R_{\mu\nu}$, square of the Ricci tensor $R = R^{\mu\nu} R_{\mu\nu}$ and the Kretschmann scalar $K = R^{\alpha\beta\mu\nu} R_{\alpha\beta\mu\nu}$ may be useful in deeply understanding the properties of a spacetime and nature of the gravity. Thus, here, we investigate the curvature invariants of the spacetime (9) around regular Bardeen BH in 4D EGB gravity. Performed calculations show that the scalar invariants have the following forms

$$\begin{aligned}
 R &= -\frac{6}{\alpha} \left[1 - \frac{\sqrt{1 + \frac{8\alpha M}{(g^2+r^2)^{\frac{3}{2}}}}}{(g^2+r^2)^2 [(g^2+r^2)^{3/2} + 8\alpha M]} \right]^2 \left\{ (g^2+r^2)^5 + 4\alpha^2 M^2 \right. \\
 &\times \left. \left(16g^4 + 14g^2r^2 + 5r^4 \right) + \frac{\alpha M}{\sqrt{g^2+r^2}} \left(16g^4 + 23g^2r^2 + 12r^4 \right) (g^2+r^2)^2 \right\}, \tag{12}
 \end{aligned}$$

$$\begin{aligned}
 \mathcal{R} = & -\frac{18}{\alpha^2(g^2+r^2)^{\frac{11}{2}}\left((g^2+r^2)^{\frac{3}{2}}+8\alpha M\right)^3}\left[\sqrt{1+\frac{8\alpha M}{(g^2+r^2)^{\frac{3}{2}}}}\left\{\left(g^2+r^2\right)^{10}\right.\right. \\
 & +\alpha M\left(g^2+r^2\right)^{\frac{7}{2}}\left[32\alpha^2 M^2\left(16g^4+14g^2r^2+5r^4\right)+\left(24g^4+39g^2r^2+20r^4\right)\right. \\
 & \times\left.\left.\left(g^2+r^2\right)^3\right]+4\alpha^2 M^2\left(48g^4+60g^2r^2+29r^4\right)\left(g^2+r^2\right)^5\right\}-\left(g^2+r^2\right)^{10} \\
 & -\alpha M\left(28g^4+47g^2r^2+24r^4\right)\left(g^2+r^2\right)^{\frac{13}{2}}-16\alpha^4 M^4\left(128g^8+224g^6r^2\right. \\
 & +228g^4r^4+100g^2r^6+17r^8)-8\alpha^3 M^3\left(160g^8+424g^6r^2+514g^4r^4\right. \\
 & +277g^2r^6+62r^8)\left(g^2+r^2\right)^{\frac{3}{2}}-\alpha^2 M^2\left(288g^8+936g^6r^2+1241g^4r^4\right. \\
 & \left.\left.+756g^2r^6+188r^8\right)\left(g^2+r^2\right)^3\right], \tag{13}
 \end{aligned}$$

$$\begin{aligned}
 K = & -\frac{12}{\alpha^2(g^2+r^2)^{\frac{11}{2}}\left((g^2+r^2)^{\frac{3}{2}}+8\alpha M\right)^3}\left[\sqrt{1+\frac{8\alpha M}{(g^2+r^2)^{\frac{3}{2}}}}\left\{32\alpha^3 M^3\right.\right. \\
 & \times\left.\left.\left(16g^4+14g^2r^2+5r^4\right)\left(g^2+r^2\right)^{\frac{7}{2}}+4\alpha^2 M^2\left(48g^4+60g^2r^2+29r^4\right)\left(g^2+r^2\right)^5\right.\right. \\
 & +\alpha M\left(24g^4+39g^2r^2+20r^4\right)\left(g^2+r^2\right)^{\frac{13}{2}}+\left.\left.\left(g^2+r^2\right)^{10}\right\}-\left(g^2+r^2\right)^{10}\right. \\
 & -16\alpha^4 M^4\left(128g^8+224g^6r^2+364g^4r^4+148g^2r^6+27r^8\right) \\
 & -\sqrt{g^2+r^2}\left[\alpha M\left(28g^4+47g^2r^2+24r^4\right)\times\left(g^2+r^2\right)^6\right. \\
 & \left.+8\alpha^3 M^3\left(160g^8+424g^6r^2+582g^4r^4+277g^2r^6+64r^8\right)\left(g^2+r^2\right)\right] \\
 & \left.-3\alpha^2 M^2\left(96g^8+312g^6r^2+425g^4r^4+248g^2r^6+64r^8\right)\left(g^2+r^2\right)^3\right]. \tag{14}
 \end{aligned}$$

When $\alpha = g = 0$, the spacetime (9) becomes Ricci flat and curvature invariants take the values $R = 0, \mathcal{R} = 0$ and $K = 48M^2/r^6$ which cover the Schwarzschild spacetime. When the radial coordinate tends to zero, the scalar invariants take the following form

$$\lim_{r \rightarrow 0} R = -\frac{6}{\alpha}\left(1-\sqrt{1+\frac{8\alpha M}{g^3}}\right), \tag{15}$$

$$\lim_{r \rightarrow 0} \mathcal{R} = \frac{18}{\alpha^2}\left(1+\frac{4\alpha M}{g^3}-\sqrt{1+\frac{8\alpha M}{g^3}}\right), \tag{16}$$

$$\lim_{r \rightarrow 0} K = \frac{12}{\alpha^2}\left(1+\frac{4\alpha M}{g^3}-\sqrt{1+\frac{8\alpha M}{g^3}}\right), \tag{17}$$

which are regular for non-zero parameters α and g . When $\alpha \rightarrow 0$ curvature invariants defined by Equations (15)–(17) remain regular, particularly, Ricci scalar at the center takes the form $R = 24 M/g^3$.

The radial dependence of the Ricci scalar (top-left panel), square of Ricci tensor (top-right panel) and Kretschmann scalar (bottom panel) of the spacetime (9) are shown in Figure 4. For convenience, we normalize all the scalar invariants and make them dimensionless. In Figure 4, we set $\alpha_{min} = -0.15$, and the unit of the GB coupling parameter

α is given in M^2 . The black solid lines in Figure 4 correspond to Schwarzschild spacetime. One can see from the figure that the presence of the magnetic charge makes the scalar invariants finite (non-zero) at the center of the BH ($r = 0$), while the presence of the parameter α causes all the scalar invariants to decrease.

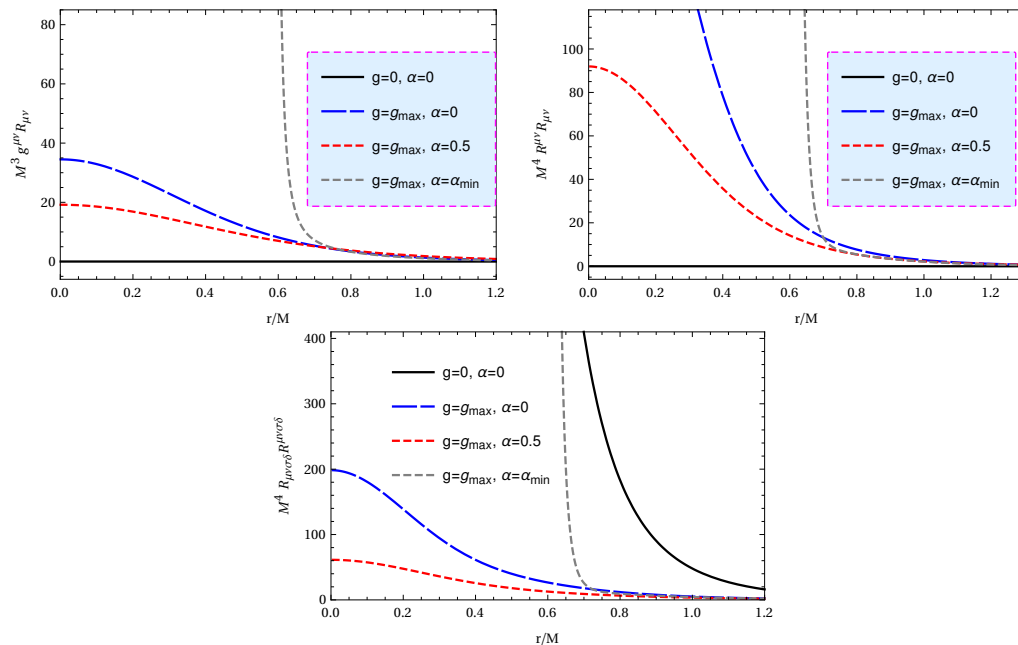


Figure 4. Dimensionless Ricci scalar (**left** panel), square of Ricci tensor (**right** panel) and Kretschmann scalar (**bottom** panel) as a function of dimensionless radial coordinate r/M for different values of the RBH parameters g and α .

3. Magnetized Particles Motion

In this section, we explore the dynamics of magnetized particle motion around the regular Bardeen BH in 4D EGB theory. Using the potential (11), one can immediately obtain the non-zero component of the electromagnetic field tensor in the form of

$$F_{\theta\phi} = -g \sin \theta, \tag{18}$$

and together with the radial orthonormal component of the magnetic field in the following form [65,69]

$$B^{\hat{r}} = \frac{g}{r^2}. \tag{19}$$

3.1. Equation of Motion

The Hamilton–Jacobi equation for magnetized particles motion around a black hole in the presence of an electromagnetic field reads [55,70]

$$g^{\mu\nu} \frac{\partial \mathcal{S}}{\partial x^\mu} \frac{\partial \mathcal{S}}{\partial x^\nu} = - \left(m - \frac{1}{2} \mathcal{D}^{\alpha\beta} F_{\alpha\beta} \right)^2, \tag{20}$$

where the interaction between magnetized particles and the magnetic field is taken into account by the term $\mathcal{D}^{\mu\nu} F_{\mu\nu}$. The polarization tensor should satisfy the following conditions,

$$\mathcal{D}^{\alpha\beta} = \eta^{\alpha\beta\sigma\nu} u_\sigma u_\nu, \quad \mathcal{D}^{\alpha\beta} u_\beta = 0, \tag{21}$$

where μ^ν is the magnetic dipole moment of the particle with the four velocity u^α and $\eta^{\alpha\beta\sigma\nu}$ is the Levi-Civita tensor. The electromagnetic field tensor $F_{\alpha\beta}$ is defined as

$$F_{\alpha\beta} = u_\alpha E_\beta - u_\beta E_\alpha - \eta_{\alpha\beta\sigma\gamma} u^\sigma B^\gamma. \tag{22}$$

Using Equations (21) and (22), one may calculate the interaction term $\mathcal{D}^{\alpha\beta} F_{\alpha\beta}$ in the following form

$$\mathcal{D}^{\alpha\beta} F_{\alpha\beta} = 2\mu_\alpha B^\alpha = 2\mu^{\hat{\alpha}} B_{\hat{\alpha}}. \tag{23}$$

Hereafter, we set the following assumption on the directions of the magnetic dipole of the magnetized particle and magnetic field of the regular Bardeen BH in 4D EGB gravity:

- We assume the direction of the magnetic dipole moment is parallel to the equatorial plane and the magnetic field. In fact, the direction of the magnetic dipole moment of the magnetized particle should be along the direction of the magnetic field lines in order to provide equilibrium in interaction with maximum energy.
- The first assumption implies that the magnetic dipole has only radial components $\mu^i = (\mu^r, 0, 0)$.
- For simplicity, the motion could be considered in the proper observer frame, which is convenient to avoid a relative motion problem.
- Again, for simplicity of calculations, the value of dipole moment magnitude is assumed to be constant.

In our preceding works [62,65,68,69], taking into account the above assumptions, we have shown that the analytical form of the interaction takes the following form

$$\mathcal{D}^{\alpha\beta} F_{\alpha\beta} = \frac{2\mu g}{r^2}. \tag{24}$$

The proper magnetic field generated by the magnetic charge of the regular Bardeen BH in 4D EGB gravity has an axial symmetric behaviour. Therefore, the specific energy and angular momentum of the magnetized particles are still conserved. We investigate the radial motion of a magnetized particle in the spacetime of a magnetically charged regular Bardeen BH in 4D EGB gravity at the equatorial plane. The effective potential for the radial motion has the following form [65,69]

$$V_{\text{eff}}(r; \mathcal{L}, \mathcal{B}, Q_m) = f(r) \left[\left(1 - \frac{\mathcal{B}}{r^2}\right)^2 + \frac{\mathcal{L}^2}{r^2} \right], \tag{25}$$

here, we introduced a new relation

$$\mathcal{B} = \frac{\mu}{m} g, \tag{26}$$

which is responsible for the magnetic interaction between the magnetized particle and the proper magnetic field. We also introduce another dimensionless non-negative parameter $\beta = \mu / (mM)$. The estimated value of β for the system of magnetized neutron star (white dwarf) having a dipolar magnetic field with $\mu = (1/2)BR^3$ orbiting around a SMBH has

$$\beta = \frac{B_{\text{NS}} R_{\text{NS}}^3}{2m_{\text{NS}} M_{\text{SMBH}}} \simeq 0.18 \left(\frac{B_{\text{NS}}}{10^{12} \text{G}} \right) \left(\frac{R_{\text{NS}}}{10^6 \text{cm}} \right) \left(\frac{m_{\text{NS}}}{M_\odot} \right)^{-1} \left(\frac{M_{\text{SMBH}}}{10^6 M_\odot} \right)^{-1}. \tag{27}$$

In Refs. [62,65,68,69], the authors have considered the magnetar SGR (PSR) J1745–2900 with magnetic dipole moment $\mu \simeq 1.6 \times 10^{32} \text{ G} \cdot \text{cm}^3$ and mass $m \simeq 1.5M_\odot$ orbiting the SMBH Sgr A* ($M \simeq 4.1 \times 10^6 M_\odot$) [71] as a test magnetized particle and obtained the value for the parameter $\beta \simeq 10.2$. Thus, in our further calculation, we fix the value of the magnetized parameter as $\beta = 10.2$.

The radial profiles of the effective potential for the radial motion of the magnetized particles with $\beta = 10.2$, around regular Bardeen BHs in 4D EGB theory are shown in Figure 5. We have fixed the particle’s angular momentum as $\mathcal{L} = 4.3M$ and the BH magnetic charge $g = 0.3$ (left panel). One can see from the figure that the positive values of the GB parameter α cause the increase in the effective potential, while the magnetic charge decreases it. It is seen from the right panel of Figure 5 that after the increase in the magnetic charge of the BH, the maximum value of the effective potential decreases due to the centrifugal repulsive behavior of the magnetic interaction.

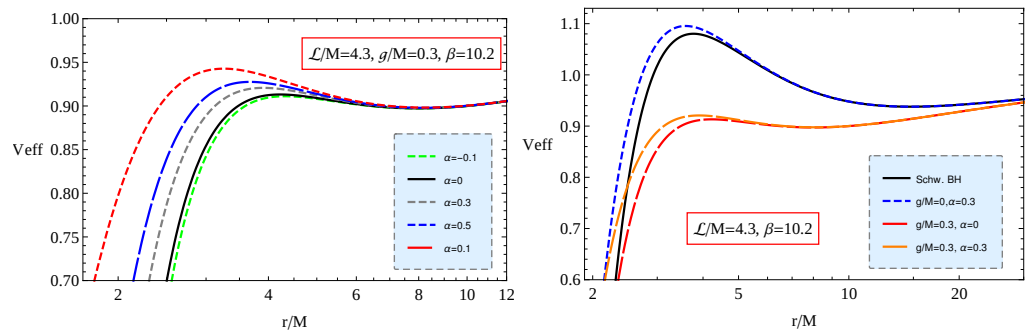


Figure 5. Radial dependence of the effective potential for radial motion of a magnetized test particle with $\beta = 10.2$ around regular BH in EDGB gravity for different values of parameter α .

3.2. Stable Circular Orbits

From the condition, $\partial_r V_{\text{eff}} = 0$, we obtain the specific angular momentum that helps to provide circular orbits for the magnetized particles. In order to find the energy of the particle along the circular orbits, we insert the obtained specific angular momentum into the effective potential given in Equation (25), and we have

$$\mathcal{L}^2 = \frac{1}{\psi(r) - \frac{2}{r^3}} \left\{ \frac{\beta g M - 2r}{2\alpha} \Psi(r) - \frac{\beta g M}{r^2} - r\psi(r)(r - \beta g M) \right\} \tag{28}$$

$$\mathcal{E}^2 = \frac{(g^2 + r^2)^{\frac{5}{2}} \sqrt{1 + \frac{8\alpha M}{(\alpha^2 + r^2)^{\frac{3}{2}}}} (2r - \beta g M)}{8\alpha^2 r \left((g^2 + r^2)^{\frac{5}{2}} \sqrt{1 + \frac{8\alpha M}{(g^2 + r^2)^{\frac{3}{2}}}} - 3Mr^4 \right)} (r^2 \Psi(r) + 2\alpha)^2 \tag{29}$$

where

$$\psi(r) = \frac{6Mr}{(g^2 + r^2)^{\frac{5}{2}} \sqrt{1 + \frac{8\alpha M}{(g^2 + r^2)^{\frac{3}{2}}}}}, \quad \Psi(r) = 1 - \sqrt{1 + \frac{8\alpha M}{(g^2 + r^2)^{\frac{3}{2}}}}.$$

Figure 6 presents the radial dependence of the specific angular momentum and energy of magnetized particles with $\beta = 10.2$, orbiting the Bardeen BH in EDGB gravity for the fixed values of magnetic charge $g = 0.3 M$ and different values of the GB parameters. One can see from Figure 6 that the presence of the negative values of the parameter α causes a slight increase in the minimum values of the energy and angular momentum, while at positives values of the BG parameter, α , they increase.

Now, we study the behavior of circular orbits; namely, we consider the innermost stable circular orbits (ISCO) radius. The equation to obtain ISCO radius can be found using the condition $\partial_{rr} V_{\text{eff}} = 0$ and inserting the expression of the angular momentum for circular orbits given in Equation (28). Due to the extra long and complicated form of the ISCO equation, here, we provide graphical analysis of the effects of the magnetic charge of the Bardeen BH and the GB parameter on the ISCO radius of magnetized particles.

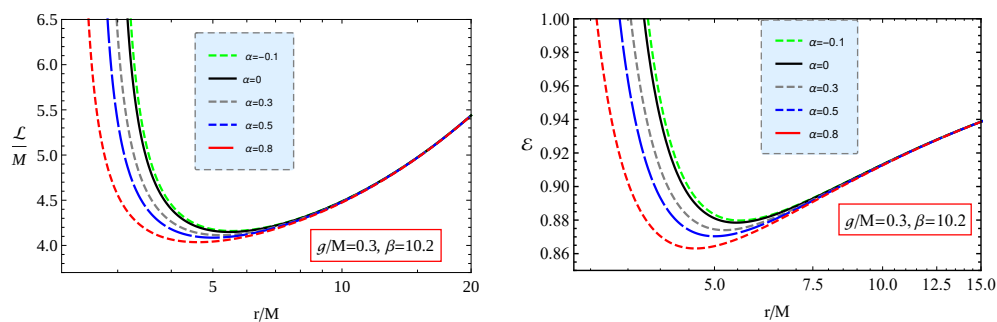


Figure 6. Radial dependence of specific angular momentum (left panel) and energy (right panel) of a magnetized test particle, with $\beta = 10.2$, along circular orbits for different values of the NED charge of the BH and coupling constant α .

Figure 7 demonstrates the ISCO radius of magnetized particles for the fixed value of the parameter $\beta = 10.2$ as a function of the magnetic charge g for the different values of the GB parameter α . It is observed from the figure that when $\alpha = g = 0$, the ISCO radius is located at the distance $6M$. One can easily see from the figure that an increase of the parameter α causes the decrease of the ISCO radius, and the decreasing rate increases with the increase of the magnetic charge. However, at the higher values of the α parameter, the minimum of the ISCO radius goes far from the central BH due to the decrease of the extreme values of the magnetic charge g .

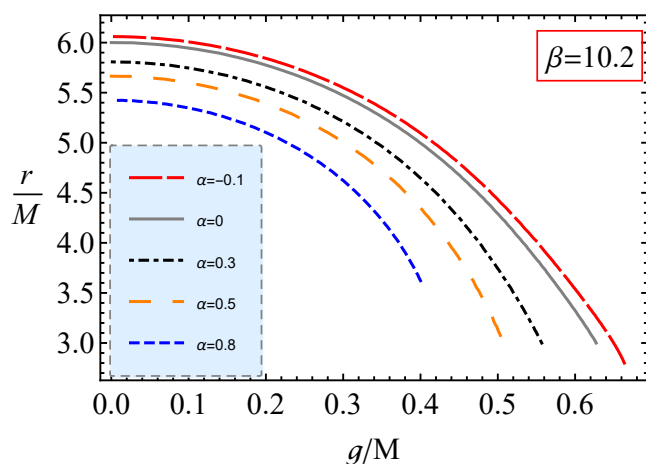


Figure 7. ISCO radius profiles of the magnetized test particle for the fixed value of the parameter $\beta = 10.2$ for different values of the NED magnetic charge and the GB coupling parameter α .

4. Magnetically Charged Particles Motion

In this section, we will explore the dynamics of a magnetically charged particle characterized by a non-vanishing magnetic monopole. Following the same logic as in the previous sections, we will construct the equation of motion. For a magnetically charged and electrically neutral particle, the Hamilton–Jacobi equation takes the form

$$g^{\alpha\beta} \left(\frac{\partial S}{\partial x^\alpha} + iq_m A_\alpha^* \right) \left(\frac{\partial S}{\partial x^\beta} + iq_m A_\beta^* \right) = -m^2, \tag{30}$$

where q_m and m are the magnetic charge and rest mass of the test particle, respectively. The Hamilton–Jacobi equation can be expanded, together with Equation (11) as

$$-\frac{1}{f(r)} \left(E - \frac{gq_m}{r} \right)^2 + \frac{L^2 \csc^2 \theta}{r^2} + \frac{1}{r^2} \left(\frac{\partial S}{\partial \theta} \right)^2 + f(r) \left(\frac{\partial S}{\partial r} \right)^2 = -m^2. \tag{31}$$

The effective potential of the radial motion of the magnetically charged particle moving at the equatorial plane, where, $\theta = \pi/2$ has the form,

$$V_{\text{eff}} = \frac{\lambda g}{r} + \sqrt{f(r) \left(1 + \frac{\mathcal{L}^2}{r^2} \right)}, \tag{32}$$

where $\lambda = q_m/m$.

In Figure 8, we have shown the radial dependence of the effective potential for the radial motion of the magnetically charged particle around a regular Bardeen BH in 4D EGB gravity for different values of the parameters λ (top panels) and α (bottom panel), and the fixed values of the magnetic charge g and the GB parameter α , respectively. One can see from the figure that in all cases, the behavior of the effective potentials are alike: rapidly growing, going away from the attractor, reaching its maximum, and then starting to smoothly decrease until it hits the constant value of kinetic energy of the particle, far away from the BH. If we consider only the vicinity of the BH, we can say that the height in maximum of the effective potential V_{eff} increases with increasing the parameter λ , and also the same for α , while the other parameters are fixed.

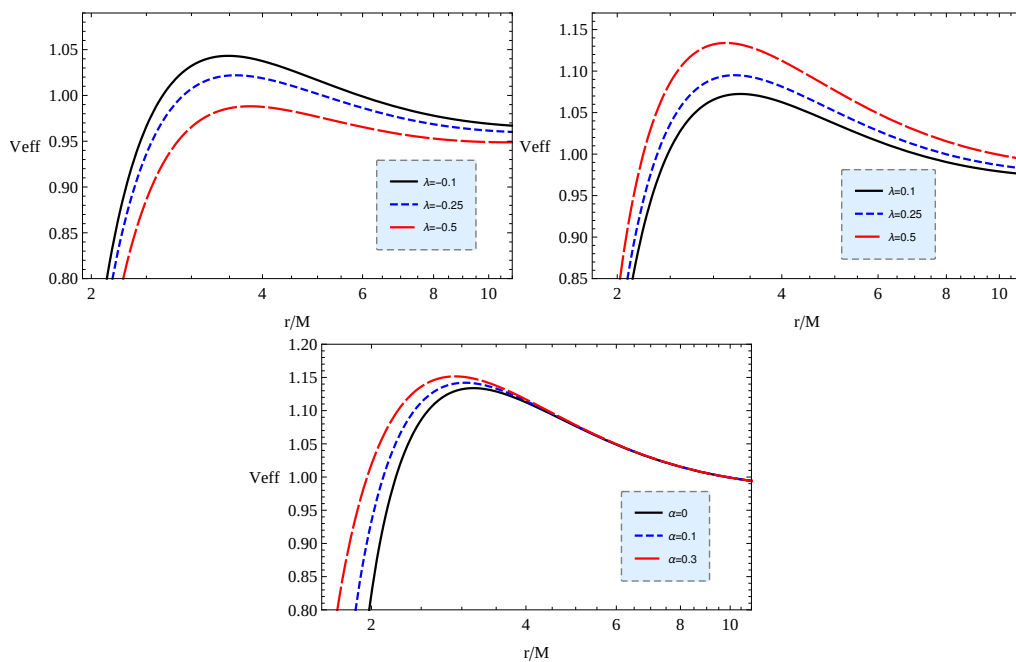


Figure 8. Effective potential dependence on radial distance for magnetically charged test particles, moving around the Bardeen regular black hole in 4D EGB gravity, possessing magnetic charge g . **Top panels:** V_{eff} against r/M for different values of negative and positive magnetic charge parameter λ in the case of fixed $g = 0.5$ and $\alpha = 0.5$. **Bottom panel:** For different values of the parameter α in the case of fixed $g = 0.5$ and $\lambda = 0.5$.

Generally, the circularity of orbits of the test magnetically charged particles around BHs is defined by the following conditions using the effective potential (32),

$$V_{\text{eff}}(r, g, \alpha, \lambda, \mathcal{L}) = \mathcal{E}, \quad V'_{\text{eff}}(r, g, \alpha, \lambda, \mathcal{L}) = 0, \tag{33}$$

where the prime denotes a derivative with respect to r . Now, one can obtain $\mathcal{E} = E/m$ and $\mathcal{L} = L/m$ of the magnetically charged particles at circular orbits using the solutions of Equation (33) in the following form

$$\mathcal{E} = \frac{\lambda g}{r} + \sqrt{f(r) \left(1 + \frac{\mathcal{L}^2}{r^2} \right)}, \tag{34}$$

$$\mathcal{L}^2 = \frac{r^4(-f'(r)^2) + 2r^3 f(r)f'(r) + 2g^2 \lambda^2 f(r)}{r^2 f'(r)^2 - 4r f(r)f'(r) + 4f(r)^2} + \frac{2\sqrt{-2g^2 \lambda^2 r^3 f(r)^2 f'(r) + 4g^2 \lambda^2 r^2 f(r)^3 + g^4 \lambda^4 f(r)^2}}{r^2 f'(r)^2 - 4r f(r)f'(r) + 4f(r)^2}. \tag{35}$$

The radial profiles of the specific angular momentum \mathcal{L} of the magnetically charged particle, circularly orbiting the BH, in different cases are illustrated in Figure 9. The top panel of this figure demonstrates profiles of \mathcal{L}^2 for different values of the parameters λ and α , while the bottom panel shows the radial dependence of the angular momentum for various values of the magnetic charge g . We can mark from Figure 9 that all the cases we tested have an innermost stable circular orbit, where the existence of its minimum is taken place. It is observed from the figure that in order for the orbits of the magnetized particles to be circular, as the value of the magnetic interaction parameter increases (an increase of both magnetic charges of the particles λ and the BH g), the particles' angular momentum should be increased. However, with the increase of g , the position where the angular momentum is minimum shifts toward the central object sufficiently with comparison to the case when λ is increased.

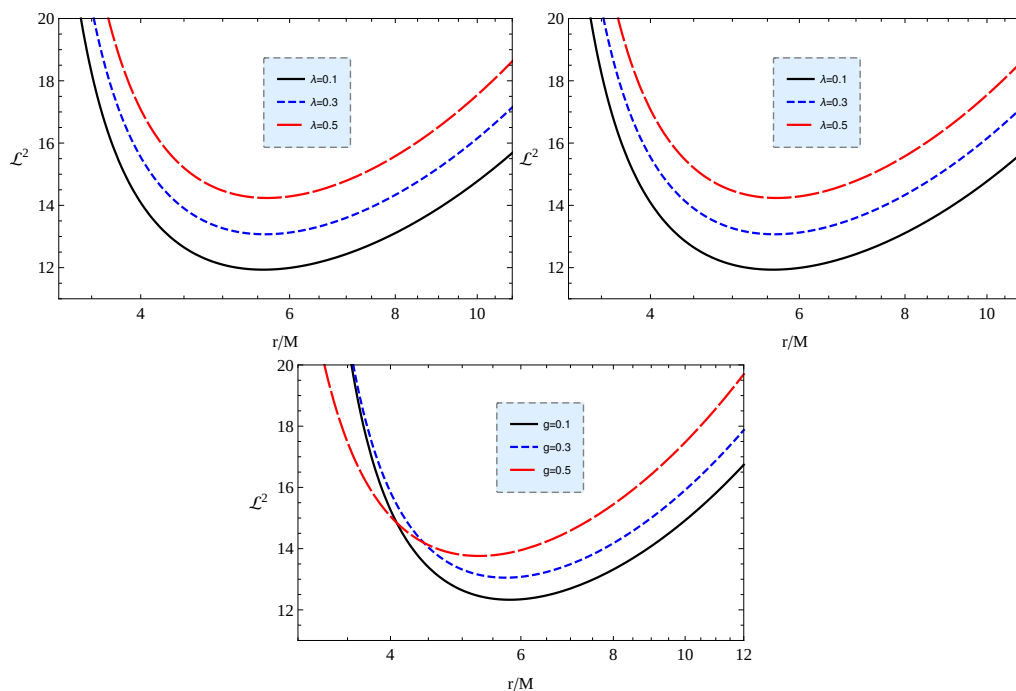


Figure 9. Angular momentum square dependence on radial distance for magnetically charged test particles, moving around the Bardeen regular black hole in 4D EGB gravity, possessing magnetic charge g . **Top** panels: \mathcal{L}^2 against r/M for different values of magnetic charge parameter λ and for the parameter α in the case of fixed $g = 0.5$. **Bottom** panel: For different values of the parameter g in the case of fixed $\alpha = 0.3$ and $\lambda = 0.5$.

First, in order to determine the ISCO position, we set up an additional condition for the second derivative of the effective potential to be zero, i.e.,

$$V''_{\text{eff}}(r, g, \alpha, \lambda, \mathcal{L}) = 0. \tag{36}$$

In fact, it is impossible to solve Equation (36) with respect to r . Therefore, in order to calculate the ISCO radii for the magnetically charged particles, we solve the equation graphically together with conditions in Equations (33) and (36).

The results derived from solutions of these equations with respect to r , for different values of the parameters α and λ , are illustrated in Figure 10. The left and right panels in this figure both present r_{ISCO} vs. g ; however, in the left panel, the parameter λ is fixed as $\lambda = 0.3$, and in the right panel, we fix the parameter $\alpha = 0.01$. It is observed from the figure that an increase of the GB parameter cause a decrease in the ISCO radius, while the BH charge g causes it to increase when $\lambda = 0.3$. However, when the values of $\lambda \ll 1$, the ISCO radius has a maximum at a critical value of the magnetic charge of the BH, while the increase of λ causes an increase in the ISCO radius.

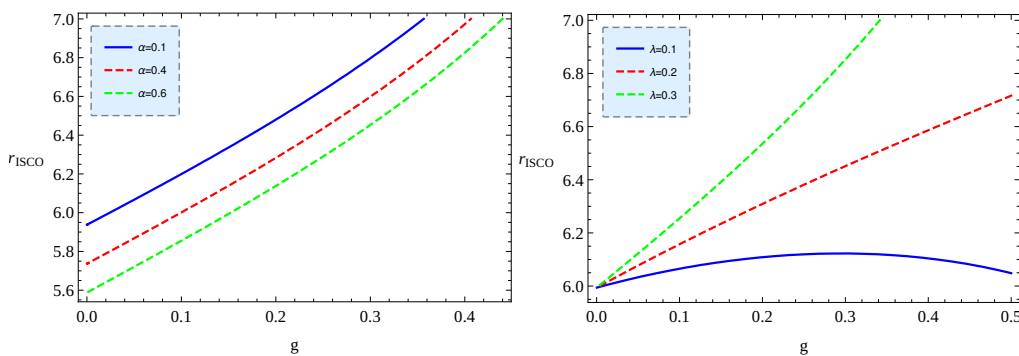


Figure 10. Innermost stable orbits dependence on magnetic charge parameter of the black hole g for different values of α , while fixing $\lambda = 0.3$ (left panel) and for different values of λ , while fixing $\alpha = 0.01$ (right panel).

5. Particles Collisions near Bardeen BH in 4D EGB Gravity

The idea and mechanism of the energy release process from BHs by the collisions of falling particles to the BHs is first developed by Banados, Silk and West in Ref. [72], where the extreme rotating Kerr BH case is explored, and it is shown that in this case, the center of mass energy of the colliding particles may be diverged.

Later, the process in the presence of external magnetic fields has been developed in Ref. [73] for the collisions of charged particles around magnetized BHs and showed that the energy extraction process becomes more effective in the case of head-on collisions.

The center-of-mass energy of collisions of two test particles can be derived by the sum of four momenta of the colliding particles in the following form [74,75],

$$\{E_{cm}, 0, 0, 0\} = m_1 u_1^\mu + m_2 u_2^\mu, \tag{37}$$

where u_i^μ is the four-velocity of the colliding particles with the mass $m_i, i = 1, 2$. The square of center-mass energy can be calculated as

$$E_{cm}^2 = m_1^2 + m_2^2 - 2m_1 m_2 g_{\mu\nu} u_1^\mu u_2^\nu. \tag{38}$$

After simple algebraic calculations, we have

$$\frac{E_{cm}^2}{m_1 m_2} = \frac{m_1}{m_2} + \frac{m_2}{m_1} - 2g_{\mu\nu} u_1^\mu u_2^\nu. \tag{39}$$

Let us assume the colliding particles have masses $m_1 = Xm$ and $m_2 = Ym$.

$$\frac{E_{cm}^2}{m^2} = X^2 + Y^2 - 2g_{\mu\nu}u_1^\mu u_2^\nu. \tag{40}$$

In this work, we explore the collisions of magnetized and magnetically charged particles near the Bardeen BH in 4D EGB gravity. For simplicity, in our further calculations, we consider that the colliding particles have the same mass; i.e., $m_1 = m_2 = m$, and their initial energies are also the same and equal to their remaining mass as $E_1 = E_2 = m$. Thus, Equation (40) takes the following form.

$$\mathcal{E}_{cm}^2 = \frac{E_{cm}^2}{4m^2c^4} = 1 - g_{\alpha\beta}u_1^\alpha u_2^\beta, \tag{41}$$

where $u_{1,2}^\alpha$ are the four velocities of the colliding particles. Now, we plan to investigate several scenarios of collisions of magnetized particles at the equatorial plane (where $\theta = \pi/2$) with magnetized, electrically (magnetically) charged, and neutral particles in the frame of the proper observer.

Four-velocities of magnetized, magnetically charged and neutral particles have the form,

$$\dot{t} = \frac{\mathcal{E}}{f(r)}, \tag{42}$$

$$\dot{r}^2 = \mathcal{E}^2 - f(r) \left[\left(1 - \beta \frac{gM}{r^2}\right)^2 + \frac{L^2}{r^2} \right], \tag{43}$$

$$\dot{\phi} = \frac{\mathcal{L}}{r^2}, \tag{44}$$

and

$$\dot{t} = \frac{1}{f(r)} \left(\mathcal{E} - \frac{\lambda g}{r} \right), \tag{45}$$

$$\dot{r}^2 = \left(\mathcal{E} - \frac{\lambda g}{r} \right)^2 - f(r) \left(1 + \frac{L^2}{r^2} \right), \tag{46}$$

$$\dot{\phi} = \frac{\mathcal{L}}{r^2}. \tag{47}$$

Correspondingly, the expression for the center-of-mass energy of the two particles takes the following form,

$$\begin{aligned} \frac{\mathcal{E}_{cm}^2}{2} &= 1 + \frac{1}{f(r)} \left(\mathcal{E}_1 - \frac{\lambda_1 g}{r} \right) \left(\mathcal{E}_2 - \frac{\lambda_2 g}{r} \right) - \frac{\mathcal{L}_1 \mathcal{L}_2}{r^2} \\ &- \frac{1}{f(r)} \sqrt{\left(\mathcal{E}_1 - \frac{\lambda_1 g}{r} \right)^2 - f(r) \left(1 + \frac{L_1^2}{r^2} \right)} \sqrt{\left(\mathcal{E}_2 - \frac{\lambda_2 g}{r} \right)^2 - f(r) \left(1 + \frac{L_2^2}{r^2} \right)}, \end{aligned} \tag{48}$$

and

$$\begin{aligned} \frac{\mathcal{E}_{cm}^2}{2} &= 1 + \frac{\mathcal{E}_1 \mathcal{E}_2}{f(r)} - \frac{\mathcal{L}_1 \mathcal{L}_2}{r^2} - \frac{1}{f(r)} \sqrt{\mathcal{E}_1^2 - f(r) \left[\left(1 - \beta_1 \frac{gM}{r^2}\right)^2 + \frac{\mathcal{L}_1^2}{r^2} \right]} \\ &\times \sqrt{\mathcal{E}_2^2 - f(r) \left[\left(1 - \beta_2 \frac{gM}{r^2}\right)^2 + \frac{\mathcal{L}_2^2}{r^2} \right]}. \end{aligned} \tag{49}$$

Note that one may use the above equations for neutral particles equalizing $\beta = 0$ and $\lambda = 0$.

5.1. Critic Angular Momentum

We assume the colliding particles motion occurs in the equatorial plane around the Bardeen BH in 4D EGB. When the collision occurs near the event horizon, the center of mass energy reaches its maximum. The angular momentum has a critical value that causes the radial velocity to be zero ($\dot{r} = 0$) [72]. The angular momentum exceeds the critical value, and the particle cannot come close to the orbits near the event horizon, while the momentum smaller than the critical value the particle falls down into the central BH.

Here, we study the critical angular momentum to test electrically neutral particles.

In Figure 11, we show the dependence of critical values of the angular momentum of test neutral particles from the GB parameter (left panel) and the magnetic charge of the BH (right panel) by varying the charge and GB parameters, respectively. One can see from this figure that larger values of the magnetic charge and the GB parameter correspond to smaller values of the angular momentum; however, the angular momentum decreases (quasi) linearly with the increase of α while the decreasing is power-law with respect to increase of the magnetic charge g .

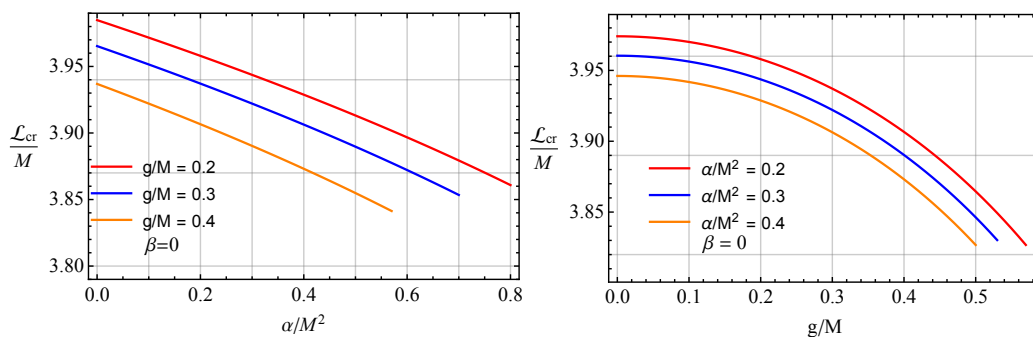


Figure 11. Figures show the dependence of the critical value of angular momentum to the α .

A similar decrease of the critical angular momentum with respect to the increase of α is also observed in the left panel of Figure 12. However, in contrast to Figure 11, it is seen from the panel that the values of the angular momentum increase with the increase of the magnetic coupling parameter β ; similarly, the increasing rate is also a power-law depending on the values of β due to the centrifugal behavior of magnetic interaction between the proper magnetic field of the Bardeen BH and the magnetic dipole of the particles.

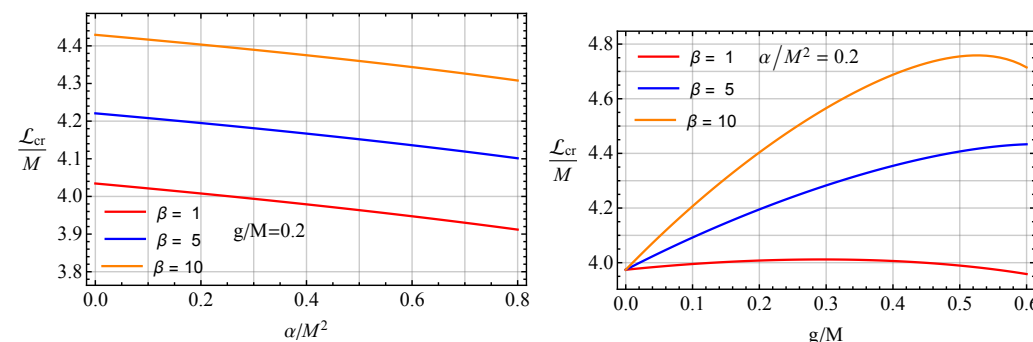


Figure 12. The same figure with Figure 11 but for magnetized particles.

It is observed from Figure 13 that an increase of the parameter λ causes a decrease of the momentum; similarly, the critical angular momentum decreases linearly with respect to the increase of the GB parameter. Moreover, one can also see that when parameter $\lambda > 0.5$, the critic value in the angular momentum increases with increasing the magnetic charge g , reaches its maximum, and then starts decreasing.

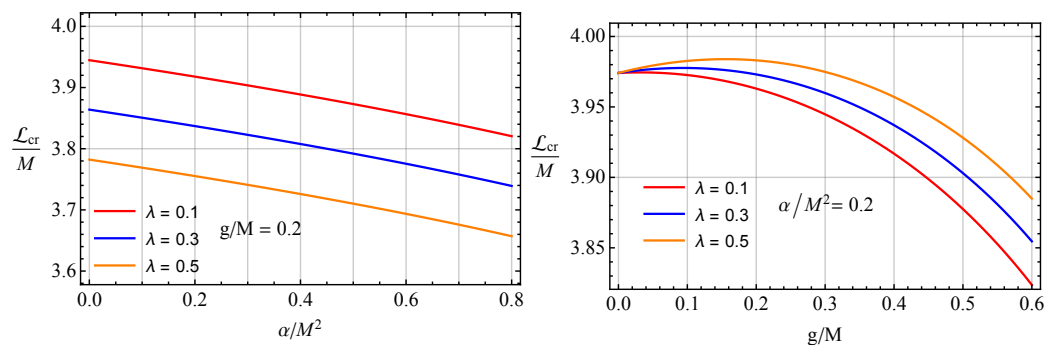


Figure 13. The same figure with Figure 11 but for magnetically charged particles.

5.2. Center of Mass Energy of Collisions of Particles

Now, we analyze the center of mass energy of colliding test particles with the critic angular momentum.

In Figure 14, we show the radial dependence of center of mass energy (\mathcal{E}_{cm}) of collisions of test electrically neutral particles around magnetically charged regular Bardeen BHs in 4D EGB gravity for different values of the GB parameter. It is seen from the figure that as the parameter α increases, the energy increases due to the event horizon coming close to the central BH.

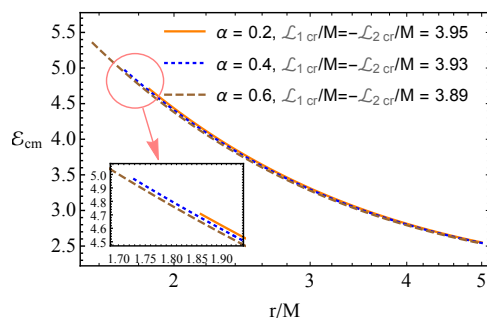


Figure 14. Radial profiles of center of mass energy of the collisions of two neutral particles with neutral particles for different values of the GB parameter and corresponding critic angular momentum.

Figure 15 shows the center of mass energy (\mathcal{E}_{cm}) of the collisions of two magnetized particles as a function of radial coordinates. Here, we obtain the magnetic charge as $g/M = 0.4$ and the GB parameter as $\alpha/M^2 = 0.2$ in the case of magnetized particles collisions with neutral particles and magnetized particles. The energy increases in collisions of test particles with magnetized particles, and the energy increases as β increases.

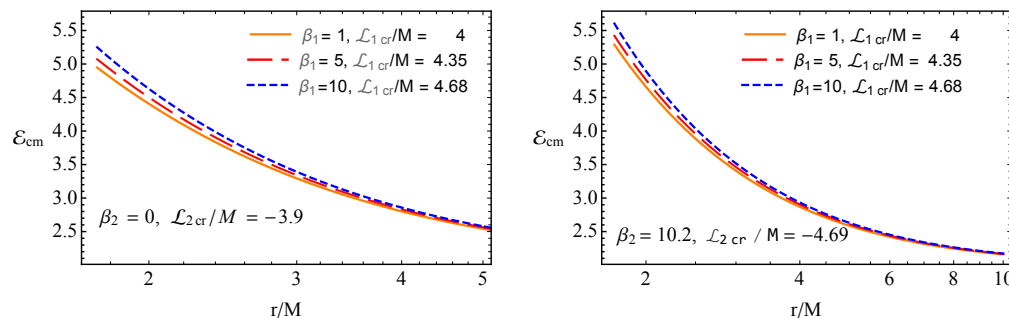


Figure 15. The same figure as Figure 14 but for collisions of two magnetized particles for different values of the GB parameter and the corresponding critic angular momentum.

Figure 16 demonstrates the behavior of the center of mass energy of head-on collisions of magnetically charged particles around the Bardeen BH, with the critical angular momentum corresponding to their parameter λ . It is seen from the figure that the presence

of the magnetic charge of the particles causes it to sufficiently decrease the energy near the horizon.

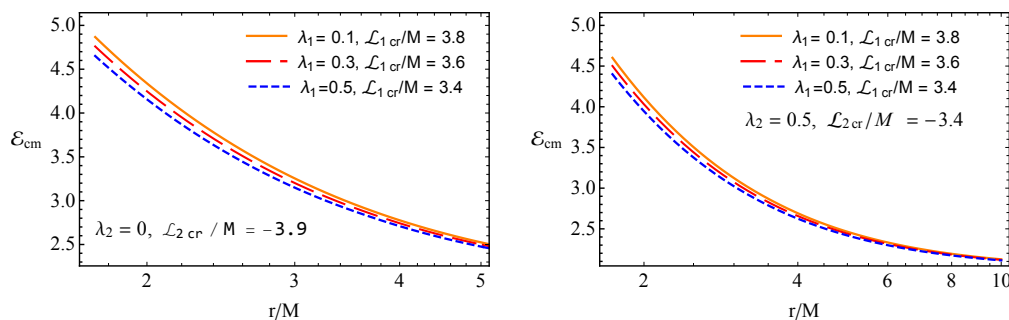


Figure 16. The same figure with Figure 14 but for collisions of magnetically charged particles with (i) neutral particles (**left** panel), and (ii) magnetically charged particles (**right** panel). Here, we choose $\alpha/M^2 = 0.2$ and $g/M = 0.4$.

In Figure 17, we show the behavior of center of mass collisions of magnetically charged and magnetized particles. It is observed from the comparisons of Figures 16 and 17 that the magnetic charge increases the center of mass energy sufficiently.

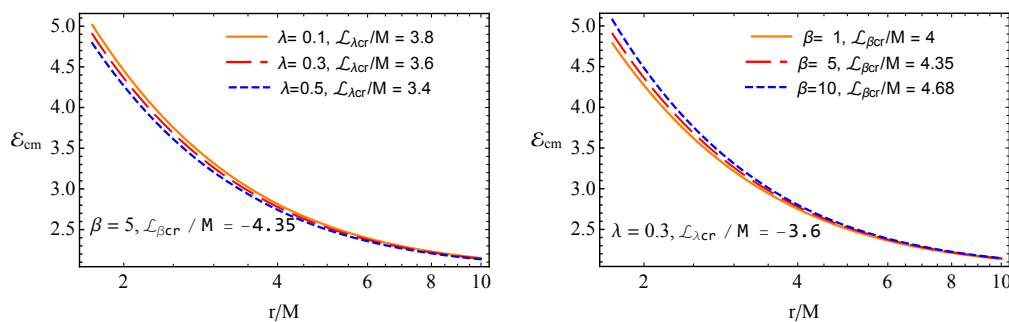


Figure 17. The same figure as Figure 14 but for collisions of magnetically charged particles with magnetized particles. Here, we choose $\alpha/M^2 = 0.2$ and $g/M = 0.4$.

6. Conclusions

The present work is devoted to the study of magnetically charged and magnetized particle dynamics around magnetically charged regular Bardeen BHs in 4D EGB theory. We have first explored properties of horizon structure and found minimum and maximum values of the GB coupling parameter as $\alpha/M \in (-0.1586, 1)$. We have also provided the space for the values of the magnetic and GB coupling parameters and divided by two the areas where the event horizon of the BH exists and does not exist. It is also shown that both the BH charge and GB parameters cause a decreasing of the outer event horizon radius. The study of curvature scalars shows that the increase of the parameter α enables the curvature scalar to grow, while the magnetic charge forces them to decrease.

We have investigated the dynamics of magnetized particles around the Bardeen BH in 4D EGB, assuming the particle’s motion occurs in the equatorial plane in the proper observation frame, and the direction of the magnetic dipole moment of the particles is always kept as radial, and the magnitude is constant. It is obtained that the minimum values of energy and angular momentum of the particles corresponding to circular orbits decrease with the increase of the GB parameter and the radius of the ISCO also decreases.

The dynamics of magnetically charged particles have also been studied and showed that both the energy and angular momentum of the particles, at circular orbits, increase with the increase of their magnetic charge. The ISCO radius of the particles also increases as the magnetic charge of the particles increases. However, the radius increases first, with respect to the increase of the BH charge, reaches its maximum, and then decreases back again.

Finally, we have studied collisions of magnetized, electrically neutral and magnetically charged particles around the Bardeen BHs in 4D EGB. We have also analyzed critical values of the angular momentum that may allow colliding the particles near the horizon radius and center of mass energy of the collisions. It is found that the critic values of the angular momentum and the center of mass energy decrease with the increase of both the BH charge and GB parameters as well as the parameter λ . Meanwhile, the presence of the magnetic charge reduces their increase.

Author Contributions: Conceptualization, J.R. and D.B.; methodology, J.R.; software, J.R. and F.A.; validation, B.A. and A.A.; formal analysis, J.R. and A.A.; investigation, A.A. and J.R. All authors have read and agreed to the published version of the manuscript.

Funding: This research is supported by Grants F-FA-2021-432, F-FA-2021-510, and MRB-2021-527 of the Uzbekistan Ministry for Innovative Development. J.R. thanks to the ERASMUS+ project 608715-EPP-1-2019-1-UZ-EPPKA2-JP (SPACECOM). D.B. thanks the Silesian University for the warm hospitality during his stay in Opava. A.A. is supported by PIFI fund of Chinese Academy of Sciences.

Data Availability Statement: Not applicable.

Conflicts of Interest: The authors declare no conflict of interest.

References

- Abbott, B.P.; Abbott, R.; Abbott, T.D.; Abernathy, M.R.; Acernese, F.; Ackley, K.; Adams, C.; Adams, T.; Addesso, P.; Adhikari, R.X.; et al. Observation of Gravitational Waves from a Binary Black Hole Merger. *Phys. Rev. Lett.* **2016**, *116*, 061102. [[CrossRef](#)] [[PubMed](#)]
- Abbott, B.P.; Abbott, R.; Abbott, T.D.; Abernathy, M.R.; Acernese, F.; Ackley, K.; Adams, C.; Adams, T.; Addesso, P.; Adhikari, R.X.; et al. Tests of General Relativity with GW150914. *Phys. Rev. Lett.* **2016**, *116*, 221101. [[CrossRef](#)] [[PubMed](#)]
- Akiyama, K. et al. [The Event Horizon Telescope Collaboration] First M87 Event Horizon Telescope Results. II. Array and Instrumentation. *Astrophys. J. Lett.* **2019**, *875*, L2. [[CrossRef](#)]
- Akiyama, K. et al. [The Event Horizon Telescope Collaboration] First M87 Event Horizon Telescope Results. III. Data Processing and Calibration. *Astrophys. J. Lett.* **2019**, *875*, L3. [[CrossRef](#)]
- Lovelock, D. The Einstein Tensor and Its Generalizations. *J. Math. Phys.* **1971**, *12*, 498–501. doi: 10.1063/1.1665613. [[CrossRef](#)]
- Glavan, D.; Lin, C. Einstein-Gauss-Bonnet Gravity in Four-Dimensional Spacetime. *Phys. Rev. Lett.* **2020**, *124*, 081301. [[CrossRef](#)]
- Malafarina, D.; Toshmatov, B.; Dadhich, N. Dust collapse in 4D Einstein-Gauss-Bonnet gravity. *arXiv* **2020**, arXiv:2004.07089.
- Zhang, C.Y.; Zhang, S.J.; Li, P.C.; Guo, M. Superradiance and stability of the novel 4D charged Einstein-Gauss-Bonnet black hole. *arXiv* **2020**, arXiv:2004.03141.
- Aguilar-Pérez, G.; Cruz, M.; Lepe, S.; Moran-Rivera, I. Hairy black hole stability under odd parity perturbations in the Einstein-Gauss-Bonnet model. *arXiv* **2019**, arXiv:1907.06168.
- Zhang, Y.P.; Wei, S.W.; Liu, Y.X. Spinning test particle in four-dimensional Einstein-Gauss-Bonnet Black Hole. *Universe* **2020**, *6*, 103.
- Guo, M.; Li, P.C. The innermost stable circular orbit and shadow in the novel 4D Einstein-Gauss-Bonnet gravity. *arXiv* **2020**, arXiv:2003.02523. [[arXiv:gr-qc/2003.02523](#)].
- Kumar, R.; Ghosh, S.G. Rotating black holes in 4D Einstein-Gauss-Bonnet gravity and its shadow. *J. Cosmol. Astropart. Phys.* **2020**, *2020*, 053. [[CrossRef](#)]
- Mishra, A.K. Quasinormal modes and Strong Cosmic Censorship in the novel 4D Einstein-Gauss-Bonnet gravity. *arXiv* **2020**, arXiv:2004.01243.
- Churilova, M.S. Quasinormal modes of the Dirac field in the novel 4D Einstein-Gauss-Bonnet gravity. *arXiv* **2020**, arXiv:2004.00513.
- Aragón, A.; Bécar, R.; González, P.A.; Vásquez, Y. Perturbative and nonperturbative quasinormal modes of 4D Einstein-Gauss-Bonnet black holes. *arXiv* **2020**, arXiv:2004.05632.
- Islam, S.U.; Kumar, R.; Ghosh, S.G. Gravitational lensing by black holes in 4D Einstein-Gauss-Bonnet gravity. *arXiv* **2020**, arXiv:2004.01038.
- Abdujabbarov, A.; Atamurotov, F.; Dadhich, N.; Ahmedov, B.; Stuchlík, Z. Energetics and optical properties of 6-dimensional rotating black hole in pure Gauss-Bonnet gravity. *Eur. Phys. J. C* **2015**, *75*, 399. [[CrossRef](#)]
- Wei, S.W.; Liu, Y.X. Testing the nature of Gauss-Bonnet gravity by four-dimensional rotating black hole shadow. *arXiv* **2020**, arXiv:2003.07769.
- Heydari-Fard, M.; Heydari-Fard, M.; Sepangi, H.R. Bending of light in novel 4D Gauss-Bonnet-de Sitter black holes by Rindler-Ishak method. *arXiv* **2020**, arXiv:2004.02140.
- Hegde, K.; Naveena Kumara, A.; Rizwan, C.L.A.; Ajith, K.M.; Sabir Ali, M. Thermodynamics, Phase Transition and Joule Thomson Expansion of novel 4-D Gauss Bonnet AdS Black Hole. *arXiv* **2020**, arXiv:2003.08778.
- Mansoori, S.A.H. Thermodynamic geometry of the novel 4-D Gauss Bonnet AdS Black Hole. *arXiv* **2020**, arXiv:2003.13382.

22. Wei, S.W.; Liu, Y.X. Extended thermodynamics and microstructures of four-dimensional charged Gauss-Bonnet black hole in AdS space. *arXiv* **2020**, arXiv:2003.14275.
23. Naveena Kumara, A.; Rizwan, C.L.A.; Hegde, K.; Sabir Ali, M.; Ajith, K.K. Rotating 4D Gauss-Bonnet black hole as particle accelerator. *arXiv* **2020**, arXiv:2004.04521.
24. Li, S.L.; Wu, P.; Yu, H. Stability of the Einstein Static Universe in 4D Gauss-Bonnet Gravity. *arXiv* **2020**, arXiv:2004.02080.
25. Abdujabbarov, A.; Rayimbaev, J.; Turimov, B.; Atamurotov, F. Dynamics of magnetized particles around 4-D Einstein Gauss-Bonnet black hole. *Phys. Dark Universe* **2020**, *30*, 100715. [[CrossRef](#)]
26. Kumar, A.; Kumar, R. Bardeen black holes in the novel 4D Einstein-Gauss-Bonnet gravity. *arXiv* **2020**, arXiv:2003.13104.
27. Gurses, M.; Cagri Sisman, T.; Tekin, B. Is there a novel Einstein-Gauss-Bonnet theory in four dimensions? *arXiv* **2020**, arXiv:2004.03390.
28. Arrechea, J.; Delhom, A.; Jiménez-Cano, A.R. Yet another comment on four-dimensional Einstein-Gauss-Bonnet gravity. *arXiv* **2020**, arXiv:2004.12998.
29. Tian, S.X.; Zhu, Z.H. Comment on “Einstein-Gauss-Bonnet Gravity in Four-Dimensional Spacetime”. *arXiv* **2020**, arXiv:2004.09954.
30. Bonifacio, J.; Hinterbichler, K.; Johnson, L.A. Amplitudes and 4D Gauss-Bonnet Theory. *arXiv* **2020**, arXiv:2004.10716.
31. Bambi, C. Testing the Kerr nature of stellar-mass black hole candidates by combining the continuum-fitting method and the power estimate of transient ballistic jets. *Phys. Rev. D* **2012**, *85*, 043002. [[CrossRef](#)]
32. Bambi, C.; Jiang, J.; Steiner, J.F. Testing the no-hair theorem with the continuum-fitting and the iron line methods: A short review. *Class. Quantum Gravity* **2016**, *33*, 064001. [[CrossRef](#)]
33. Zhou, M.; Cao, Z.; Abdikamalov, A.; Ayzenberg, D.; Bambi, C.; Modesto, L.; Nampalliwar, S. Testing conformal gravity with the supermassive black hole in 1H0707-495. *Phys. Rev. D* **2018**, *98*, 024007. [[CrossRef](#)]
34. Tripathi, A.; Yan, J.; Yang, Y.; Yan, Y.; Garnham, M.; Yao, Y.; Li, S.; Ding, Z.; Abdikamalov, A.B.; Ayzenberg, D.; et al. Constraints on the spacetime metric around seven “bare” AGN using X-ray reflection spectroscopy. *arXiv* **2019**, arXiv:1901.03064.
35. Bambi, C. *Black Holes: A Laboratory for Testing Strong Gravity*; Springer: Singapore, 2017.
36. Chandrasekhar, S. *The Mathematical Theory of Black Holes*; Oxford University Press: New York, NY, USA, 1998.
37. Wald, R.M. Black hole in a uniform magnetic field. *Phys. Rev. D* **1974**, *10*, 1680–1685. [[CrossRef](#)]
38. Aliev, A.N.; Galtsov, D.V.; Petukhov, V.I. Negative absorption near a magnetized black hole—Black hole masers. *Astrophys. Space Sci.* **1986**, *124*, 137–157. [[CrossRef](#)]
39. Aliev, A.N.; Gal'tsov, D.V. REVIEWS OF TOPICAL PROBLEMS: “Magnetized” black holes. *Sov. Phys. Uspekhi* **1989**, *32*, 75–92. [[CrossRef](#)]
40. Aliev, A.N.; Özdemir, N. Motion of charged particles around a rotating black hole in a magnetic field. *Mon. Not. R. Astron. Soc.* **2002**, *336*, 241–248. [[CrossRef](#)]
41. Stuchlík, Z.; Schee, J.; Abdujabbarov, A. Ultra-high-energy collisions of particles in the field of near-extreme Kehagias-Sfetsos naked singularities and their appearance to distant observers. *Phys. Rev. D* **2014**, *89*, 104048. [[CrossRef](#)]
42. Abdujabbarov, A.; Ahmedov, B. Test particle motion around a black hole in a braneworld. *Phys. Rev. D* **2010**, *81*, 044022. [[CrossRef](#)]
43. Abdujabbarov, A.; Ahmedov, B.; Hakimov, A. Particle motion around black hole in Hořava-Lifshitz gravity. *Phys. Rev. D* **2011**, *83*, 044053. [[CrossRef](#)]
44. Abdujabbarov, A.A.; Ahmedov, B.J.; Shaymatov, S.R.; Rakhmatov, A.S. Penrose process in Kerr-Taub-NUT spacetime. *Astrophys. Space Sci.* **2011**, *334*, 237–241. [[CrossRef](#)]
45. Abdujabbarov, A.A.; Ahmedov, B.J.; Kagramanova, V.G. Particle motion and electromagnetic fields of rotating compact gravitating objects with gravitomagnetic charge. *Gen. Relativ. Gravit.* **2008**, *40*, 2515–2532. [[CrossRef](#)]
46. Stuchlík, Z.; Kološ, M. Acceleration of the charged particles due to chaotic scattering in the combined black hole gravitational field and asymptotically uniform magnetic field. *Eur. Phys. J. C* **2016**, *76*, 32. [[CrossRef](#)]
47. Kovář, J.; Kopáček, O.; Karas, V.; Stuchlík, Z. Off-equatorial orbits in strong gravitational fields near compact objects II: Halo motion around magnetic compact stars and magnetized black holes. *Class. Quantum Gravity* **2010**, *27*, 135006. [[CrossRef](#)]
48. Kovář, J.; Slaný, P.; Cremaschini, C.; Stuchlík, Z.; Karas, V.; Trova, A. Electrically charged matter in rigid rotation around magnetized black hole. *Phys. Rev. D* **2014**, *90*, 044029. [[CrossRef](#)]
49. Rayimbaev, J.; Tadjimuratov, P. Can modified gravity silence radio-loud pulsars? *Phys. Rev. D* **2020**, *102*, 024019. [[CrossRef](#)]
50. Rayimbaev, J.; Turimov, B.; Palvanov, S. Plasma magnetosphere of slowly rotating magnetized neutron star in braneworld. *Int. J. Mod. Phys. Conf. Ser.* **2019**, *49*, 1960019. [[CrossRef](#)]
51. Rayimbaev, J.; Turimov, B.; Marcos, F.; Palvanov, S.; Rakhmatov, A. Particle acceleration and electromagnetic field of deformed neutron stars. *Mod. Phys. Lett. A* **2020**, *35*, 2050056. [[CrossRef](#)]
52. Rayimbaev, J.; Turimov, B.; Ahmedov, B. Braneworld effects in plasma magnetosphere of a slowly rotating magnetized neutron star. *Int. J. Mod. Phys. D* **2019**, *28*, 1950128. [[CrossRef](#)]
53. Stuchlík, Z.; Kološ, M.; Kovář, J.; Slaný, P.; Tursunov, A. Influence of Cosmic Repulsion and Magnetic Fields on Accretion Disks Rotating around Kerr Black Holes. *Universe* **2020**, *6*, 26. [[CrossRef](#)]
54. Stuchlík, Z.; Kološ, M.; Tursunov, A. Penrose Process: Its Variants and Astrophysical Applications. *Universe* **2021**, *7*, 416. [[CrossRef](#)]
55. de Felice, F.; Sorge, F. Magnetized orbits around a Schwarzschild black hole. *Class. Quantum Gravity* **2003**, *20*, 469–481. [[CrossRef](#)]

56. de Felice, F.; Sorge, F.; Zilio, S. Magnetized orbits around a Kerr black hole. *Class. Quantum Gravity* **2004**, *21*, 961–973. [[CrossRef](#)]
57. Rayimbaev, J.R. Magnetized particle motion around non-Schwarzschild black hole immersed in an external uniform magnetic field. *Astrophys. Space Sci.* **2016**, *361*, 288. [[CrossRef](#)]
58. Toshmatov, B.; Abdujabbarov, A.; Ahmedov, B.; Stuchlík, Z. Motion and high energy collision of magnetized particles around a Hořava-Lifshitz black hole. *Astrophys. Space Sci.* **2015**, *360*, 19. [[CrossRef](#)]
59. Abdujabbarov, A.; Ahmedov, B.; Rahimov, O.; Salikhbaev, U. Magnetized particle motion and acceleration around a Schwarzschild black hole in a magnetic field. *Phys. Scr.* **2014**, *89*, 084008. [[CrossRef](#)]
60. Rahimov, O.G.; Abdujabbarov, A.A.; Ahmedov, B.J. Magnetized particle capture cross section for braneworld black hole. *Astrophys. Space Sci.* **2011**, *335*, 499–504. [[CrossRef](#)]
61. Haydarov, K.; Rayimbaev, J.; Abdujabbarov, A.; Palvanov, S.; Begmatova, D. Magnetized particle motion around magnetized Schwarzschild-MOG black hole. *Eur. Phys. J. C* **2020**, *80*, 399. [[CrossRef](#)]
62. Narzilloev, B.; Rayimbaev, J.; Shaymatov, S.; Abdujabbarov, A.; Ahmedov, B.; Bambi, C. Can the dynamics of test particles around charged stringy black holes mimic the spin of Kerr black holes? *Phys. Rev. D* **2020**, *102*, 044013. [[CrossRef](#)]
63. Rayimbaev, J.; Figueroa, M.; Stuchlík, Z.; Juraev, B. Test particle orbits around regular black holes in general relativity combined with nonlinear electrodynamics. *Phys. Rev. D* **2020**, *101*, 104045. [[CrossRef](#)]
64. Turimov, B.; Rayimbaev, J.; Abdujabbarov, A.; Ahmedov, B.; Stuchlík, Z.C.V. Test particle motion around a black hole in Einstein-Maxwell-scalar theory. *Phys. Rev. D* **2020**, *102*, 064052. [[CrossRef](#)]
65. Vrba, J.; Abdujabbarov, A.; Kološ, M.; Ahmedov, B.; Stuchlík, Z.; Rayimbaev, J. Charged and magnetized particles motion in the field of generic singular black holes governed by general relativity coupled to nonlinear electrodynamics. *Phys. Rev. D* **2020**, *101*, 124039. [[CrossRef](#)]
66. Vrba, J.; Abdujabbarov, A.; Tursunov, A.; Ahmedov, B.; Stuchlík, Z. Particle motion around generic black holes coupled to non-linear electrodynamics. *Eur. Phys. J. C* **2019**, *79*, 778. [[CrossRef](#)]
67. Bardeen, J. Non-singular general-relativistic gravitational collapse. In Proceedings of the GR5, Tbilisi, Georgia, 9–13 September 1968; DeWitt, C., DeWitt, B., Eds.; Gordon and Breach: Tbilisi, Georgia, 1968; p. 174.
68. Narzilloev, B.; Rayimbaev, J.; Shaymatov, S.; Abdujabbarov, A.; Ahmedov, B.; Bambi, C. Dynamics of test particles around a Bardeen black hole surrounded by perfect fluid dark matter. *Phys. Rev. D* **2020**, *102*, 104062. [[CrossRef](#)]
69. Juraeva, N.; Rayimbaev, J.; Abdujabbarov, A.; Ahmedov, B.; Palvanov, S. Distinguishing magnetically and electrically charged Reissner–Nordström black holes by magnetized particle motion. *Eur. Phys. J. C* **2021**, *81*, 124078. [[CrossRef](#)]
70. Rayimbaev, J.; Abdujabbarov, A.; Jamil, M.; Han, W.B. Dynamics of magnetized particles around Einstein-Æther black hole with uniform magnetic field. *Nucl. Phys. B* **2021**, *966*, 115364. [[CrossRef](#)]
71. Mori, K.; Gotthelf, E.V.; Zhang, S.; An, H.; Baganoff, F.K.; Barrière, N.M.; Beloborodov, A.M.; Boggs, S.E.; Christensen, F.E.; Craig, W.W.; et al. NuSTAR Discovery of a 3.76 s Transient Magnetar Near Sagittarius A*. *Astron. J. Lett.* **2013**, *770*, L23. [[CrossRef](#)]
72. Bañados, M.; Silk, J.; West, S.M. Kerr Black Holes as Particle Accelerators to Arbitrarily High Energy. *Phys. Rev. Lett.* **2009**, *103*, 111102. [[CrossRef](#)]
73. Frolov, V.P. Weakly magnetized black holes as particle accelerators. *Phys. Rev. D* **2012**, *85*, 024020. [[CrossRef](#)]
74. Grib, A.A.; Pavlov, Y.V. On particle collisions near rotating black holes. *Gravit. Cosmol.* **2011**, *17*, 42–46. [[CrossRef](#)]
75. Grib, A.A.; Pavlov, Y.V. On particle collisions in the gravitational field of the Kerr black hole. *Astropart. Phys.* **2011**, *34*, 581–586. [[CrossRef](#)]